ARTICLE

Covalently Combining Carbon Nanotubes with Anticancer Agent: Preparation and Antitumor Activity

Wei Wu,[†] Rutian Li,[‡] Xiaochen Bian,[§] Zhenshu Zhu,[†] Dan Ding,[†] Xiaolin Li,[‡] Zhijun Jia,[∥] Xiqun Jiang,[†,*] and Yiqiao Hu[§]

[†]Laboratory of Mesoscopic Chemistry and Department of Polymer Science & Engineering, College of Chemistry & Chemical Engineering, Nanjing University, Nanjing 210093, People's Republic of China, [‡]Comprehensive Cancer Center of Drum Tower Hospital, Medical School of Nanjing University & Clinical Cancer Institute, Nanjing University, Nanjing 210008, People's Republic of China, [§]Department of Biochemistry, College of Life Science, Nanjing University, Nanjing 210093, People's Republic of China, and [∥]Department of Nuclear Medicine, Drum Tower Hospital Affiliated with Nanjing University, Nanjing 210008, People's Republic of China

ABSTRACT A multiwalled carbon nanotube (MWNT)-based drug delivery system was developed by covalently combining carbon nanotubes with the antitumor agent 10-hydroxycamptothecin (HCPT) using hydrophilic diaminotriethylene glycol as the spacer between nanotube and drug moieties. The surface functionalizations of the nanotube were carried out by enrichment of carboxylic groups with optimized oxidization treatment, followed by covalently linking hydrophilic diaminotriethylene glycol *via* amidation reaction, and then HCPT was chemically attached to carbon nanotubes through a cleavable ester linkage. It is demonstrated that the obtained MWNT—HCPT conjugates are superior in antitumor activity both *in vitro* and *in vivo* to clinical HCPT formulation. *In vivo* single photon emission computed tomography (SPECT) imaging and *ex vivo* gamma scintillation counting analyses reveal that MWNT—HCPT conjugates have relatively long blood circulation and high drug accumulation in the tumor site. These properties together with the enhanced cell uptake and multivalent presentation of HCPT on a single nanotube benefit substantially the antitumor effects and would boost significantly the applications of carbon nanotubes in the biomedicine field.

KEYWORDS: carbon nanotubes · drug delivery · 10-hydroxycamptothecin · antitumor performance · biodistribution

Carbon nanotubes (CNTs) have been investigated as an excellent candidate for drug delivery carrier due to their quasi-one-dimensional nanostructure, unique optical and electronic properties, ultrahigh surface area, remarkable cell membrane penetrability, and facile functionalization by different ways.[1−17] This application potential has been arousing increasing concerns for the biocompatibility of carbon nanotubes. With respect to other inorganic nanomaterials, the composition of full carbon of carbon nanotubes greatly benefits their biocompatibility. Although the metal contaminations derived from the catalysts and the aggregation of hydrophobic carbon nanotubes may conduce some extent of toxicity, this toxicity can be efficiently diminished by purification and hydrophilic modification treatments.[1,2,18,19] So far, it has been generally acknowledged that well-functionalized hydrophilic carbon nanotubes exhibit good biocompatibility.[1] However, in living system, CNT-related carriers are generally susceptible to the opsonization-induced reticuloendothelial system (RES) uptake, which attenuates significantly their retention time in the bloodstream and eventual bioavailability of the carried drug. To address this issue, PEGylation has been considered as a useful way for such carriers to resist opsonization and acquire long circulation *in vivo*.[1,2,18,20−23] Although poly(ethylene glycol) (PEG) does exhibit remarkable advantages, such as high hydrophilicity, good biocompatibility, and low immunogenicity, its intrinsic drawbacks have also been progressively revealed. For example, PEG can activate the complement system in a molecular weight (MW)- and concentration-dependent manner. Briefly, increasing either the MW or concentration of PEG would evidently accelerate the complement activation.[24] The complement activation may cause the release of anaphylatoxins, which is thought to be responsible for the observed pseudoallergic reaction following intravenous injections of PEG-containing medicines.[24−26] Furthermore, it has been revealed that the PEG coating can block the interaction between CNTs and cells and consequently affect the cellular uptake of CNTs, which is also closely related to the MW and surface density of PEG and greatly unfavorable to the therapeutic function of the carried drug.[27,28] Summarily, the longer PEG chain may accelerate complement activation and incur weak cellular uptake to a greater extent in spite of their longer circulation. Thus, rationally designed functionalization schemes are

*Address correspondence to jiangx@nju.edu.cn.

Received for review May 30, 2009 and accepted August 14, 2009.

Published online August 24, 2009. 10.1021/nn9005686 CCC: $40.75

important to balance such contradictive factors for developing the effective CNT-based carriers. In addition, the linking manner of drug to CNTs is also important for the overall performance of the conjugates. Up to now, diverse antitumor drugs have been loaded onto CNTs *via* covalent or noncovalent means.[2−6,8,16] Pastorin *et al.* attached both methotrexate and fluorescein isothiocyanate (FITC) onto the side wall of MWNTs *via* the 1,3-dipolar cycloaddition reaction of azomethine ylides and found that the functionalized MWNTs could be internalized by Jurkat cells, but no further evaluation of the antitumor activity and other biological property of the functionalized MWNTs was presented.[16] Bhirde *et al.* combined both cisplatin and epidermal growth factor (EGF, as a targeting agent to squamous cancer) with SWNTs *via* the coordination and amidation of nanotube-bound carboxylic groups, respectively, and found that the system had good *in vitro* and *in vivo* antitumor activity except that the drug loading was low (~5.2 μmol/g).[6] Besides these two examples, noncovalent means (including hydrophobic or π−π stacking interactions) were mostly used to load the antitumor drug.[2−5,8] Since the noncovalent interaction is not as robust as covalent linkage, the early release of the drug before reaching the pharmacologic tissues should be inevitable. Conclusively, the CNT-based carriers with good biocompatibility, efficient cellular uptake, long circulation time, and appropriate drug-linking manner are in demand for the further development of CNTs in the biomedical application field.

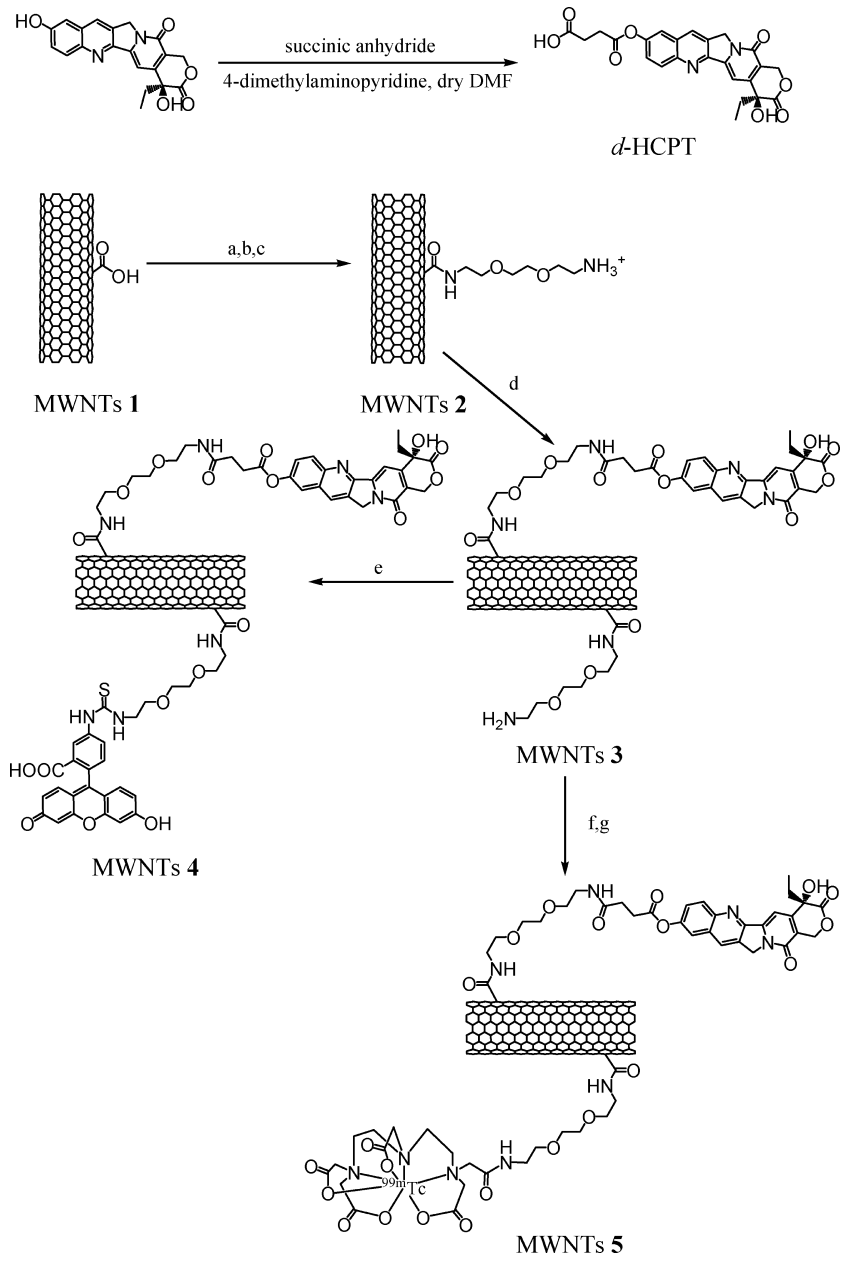

Scheme 1. Synthesis route of the MWNT−HCPT conjugates. (a) Thionyl chloride, reflux; (b) Boc-NH$(CH_2CH_2O)_2$-$CH_2CH_2NH_2$, triethylamine, anhydrous THF, reflux; (c) 4 M HCl in dioxane; (d) *d*-HCPT, EDC × HCl, NHS, triethylamine, anhydrous DMF; (e) FITC, anhydrous DMF; (f) DTPA dianhydride, triethylamine, anhydrous DMSO; (g) stannous chloride, $^{99m}TcO_4^-$.

Herein, we report the preparation and antitumor activity of a multiwalled carbon nanotube (MWNT)-based drug delivery system, in which the antitumor agent 10-hydroxycamptothecin (HCPT) is covalently linked with the MWNT by a hydrophilic spacer of diaminotriethylene glycol through biocleavable ester linkage (Scheme 1). Being similar to its congeners, such as camptothecin (CPT), 7-ethyl-10-hydroxycamptothecin (SN-38), and so on, HCPT displays a prominent therapeutic role to a broad spectrum of tumors by inhibiting the DNA enzyme topoisomerase I.[29,30] However, the inherent poor solubility of HCPT in aqueous medium greatly limits its clinical applications. We anticipate that combining HCPT with CNTs through a hydrophilic oligomeric ethylene glycol in a biocleavable linking manner can improve its aqueous solubility and simultaneously endow the drug with efficient cellular uptake, long blood circulation, and eventual high antitumor activity. Encouragingly, these desired properties are essentially exhibited by the obtained MWNT−HCPT conjugates in the current work.

RESULTS AND DISCUSSION

Synthesis of MWNT−HCPT Conjugates. Scheme 1 summarizes the entire synthesis route of the MWNT−HCPT conjugates. The high hydrophobic and metal catalyst-

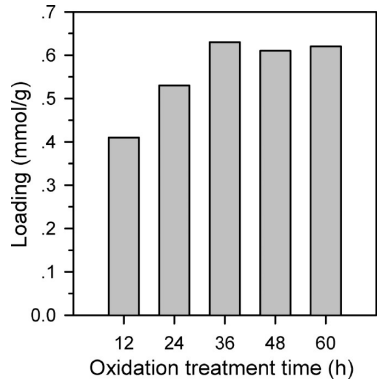

Figure 1. Loadings of the MWNTs treated by different oxidation times. The values were obtained by a quantitative Kaiser test after introduction of amine *via* nanotube-bound carboxylic groups.

containing features of pristine CNTs depress greatly their biological security and consequently hamper their application potential in biomedicine fields. To surmount these obstacles, purification and hydrophilic modification were performed. Oxidation treatment, as an effective approach to eliminate the contaminants and concomitantly generate abundant carboxylic groups at the defect sites of CNTs, was adopted as the primary step to synthesize the target product of MWNT−HCPT conjugates in the current work.

For the purpose of increasing the amount of MWNT-bound carboxylic groups and improving MWNTs' water solubility as well as capacity to conjugate drugs, a series of oxidized MWNTs were prepared by varying the duration of oxidation treatment from 12 to 60 h with a 12 h interval in a mixture of sulfuric and nitric acids under the sonication. The loadings (amount of functional groups) in CNT were measured following essentially the procedures reported previously.[17] The CNT-bound carboxylic groups preactivated as acyl chlorides were derivatived with *tert*-butyloxycarbonyl (Boc) group monoprotected diaminotriethylene glycol through amidation, followed by the cleavage of the Boc groups (see Supporting Information for detailed experimental procedures). The amount of the obtained free amino groups on the CNT sample was counted with a quantitative Kaiser test. As shown in Figure 1, the amount of amino groups on the CNT sample increases with the elongation of the oxidation treatment from 0.41 mmol/g for 12 h to 0.63 mmol/g for 36 h, whereas when the oxidation time exceeds 36 h, the loading tends to be a constant approximately. These loading results are obviously different from those reported previously,[17] which can be ascribed reasonably to the difference in the structure of CNTs used (*e.g.*, diameter and especially defect content). The MWNTs treated by 36 h oxidation were selected for subsequent synthesis and named as MWNTs **1** (Scheme 1). The length of MWNTs **1** is in the range of 20−700 nm with a mean of ~160 nm, as statistically estimated by scanning electronic microscopy (SEM, Figure 2). Furthermore, to determine

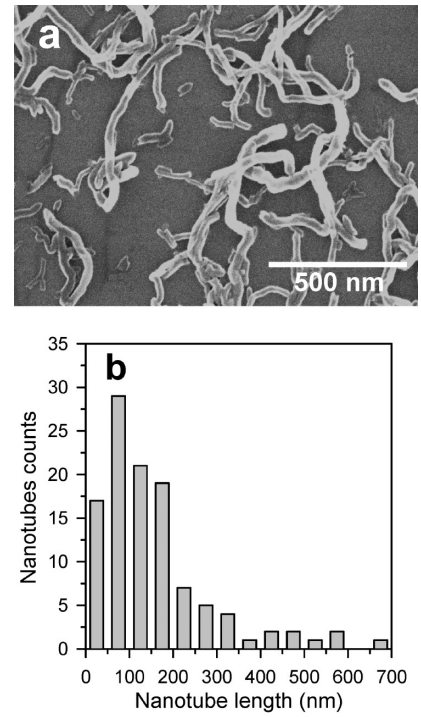

Figure 2. (a) Typical SEM image of MWNTs 1. (b) Length distribution histogram of MWNTs 1 measured *via* the SEM image.

whether there are still the metal elements derived from the catalysts (containing Fe, Y, and La metal elements) in MWNTs **1**, X-ray photoelectron spectroscopy (XPS) analyses were performed (see Figure S1 in Supporting Information for the XPS spectra of MWNTs **1**). No detectable metal element is found in the sample of MWNTs **1**, which would greatly benefit their action as drug carriers.

To couple HCPT with MWNTs, a succinate-based HCPT ester derivative (*d*-HCPT, Scheme 1) was initially synthesized through the 10-hydroxy group, which was structurally characterized by UV−vis spectroscopy, ^{1}H, ^{13}C nuclear magnetic resonance (NMR), and electrospray ionization (ESI) mass spectroscopy (detailed in Supporting Information). Thereafter, the *d*-HCPT was linked to MWNTs *via* two synthesis stages. First, the amino groups were introduced to MWNTs **1** following described procedures, giving MWNTs **2** (Scheme 1). The obtained MWNTs **2** exhibit an amino group amount of ~0.63 mmol/g as determined by a quantitative Kaiser test. Second, *d*-HCPT activated previously with *N*-(3-dimethylaminopropyl)-*N*′-ethylcarbodiimide hydrochloride (EDC × HCl) and *N*-hydroxysuccinimide (NHS) was attached to the surface of MWNTs **2** *via* amidation, affording MWNTs **3** (Scheme 1). After removing the unconjugated *d*-HCPT thoroughly by filtration (monitored by thin-layer chromatography), the specific linkage of *d*-HCPT to MWNTs was confirmed by the UV−vis spectrum (Figure 3a). In the spectrum of MWNTs **3**, the typical absorption bands from *d*-HCPT can be observed. After subtraction of the contribution of CNTs to the ab-

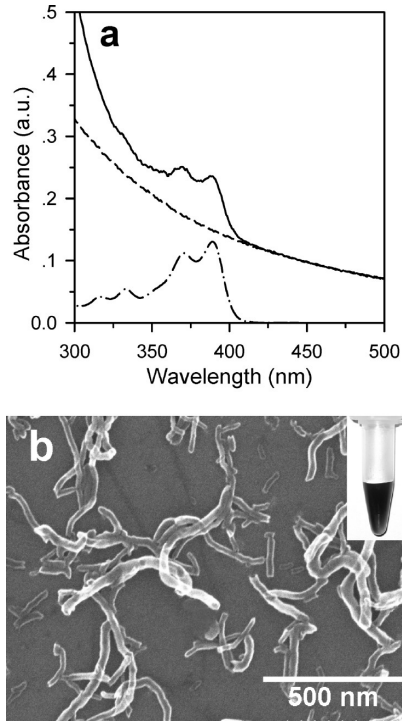

Figure 3. (a) UV−vis spectra of MWNTs 3 (solid line), MWNTs 2 (dashed line), and *d*-HCPT (dash-dot line) in DMSO. (b) Typical SEM image of MWNTs 3. Inset shows a photograph of MWNTs 3 solution in saline.

sorbance, the loading of HCPT was evaluated to be ~16% on the basis of the calibration curve, indicating that a satisfactory drug loading content is achieved by this strategy. In addition, according to the quantitative Kaiser test, the amount of free amino groups on MWNTs changed from ~0.63 to ~0.13 mmol/g after the conjugation of *d*-HCPT, which corroborated the drug loading determined by UV−vis. MWNTs **3** are quite soluble in aqueous medium, as indicated by the inset image of Figure 3b, which is attributable to the high density of the hydrophilic glycol chains on the surface of MWNTs (every ~120 nanotube carbon atoms for one chain based on the quantitative Kaiser test, regardless of the layer number of MWNTs). The morphology of MWNTs **3** was analyzed by SEM (Figure 3b). No detectable change was found in comparison with that of MWNTs **1**.

***In Vitro* Performance of the MWNT−HCPT Conjugates.** Since the ester bond used to link the nanotube and drug moieties is hydrolytically unstable, the nanotube-carried HCPT should be released in an aqueous environment to some extent. Figure 4 shows the *in vitro* HCPT release profiles of MWNTs **3** in buffer solutions with different pH values and fetal bovine serum (FBS) at 37 °C. It can be seen that HCPT release is faster at pH 5.0 than at pH 7.4 in buffer solutions within 128 h monitoring duration. However, the released portion did not exceed 15% of the total amount of loaded drug during the experiment period at either pH 5.0 or 7.4, indicating relatively high stability of the ester bond in the absence of enzyme. By contrast, a much faster release can be found

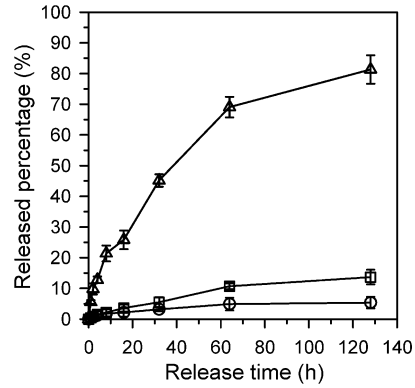

Figure 4. *In vitro* release profiles of MWNTs 3 in the media of phosphate buffered saline (pH 7.4, 0.1 M, circle), acetate buffered saline (pH 5.0, 0.1 M, square), and fetal bovine serum (triangle) at 37 °C, expressed as the percentage of cumulative release to the total amount of HCPT in the sample.

in FBS, which is attributable to the catalysis of the esterase in serum on the hydrolysis of ester linkage.

Laser scanning confocal microscopy (LSCM) was used to trace the cellular uptake of the MWNT−HCPT labeled with FITC through the remnant amino groups (MWNTs **4**, Scheme 1). Figure 5 shows the section image of human gastric carcinoma MKN-28 cells co-incubated with MWNTs **4** at 37 °C for 2 h. It can be seen that, after being incubated with MWNTs **4**, cells still maintain their normal morphology, and MWNTs **4** are distributed in the entire cell cytoplasm, with a little in nuclear, suggesting that MWNT−HCPT has great ability to penetrate cell membrane barriers and localizes in cell cytoplasm. This is crucial to exert the pharmacological activity of HCPT on the basis of the acting mechanism of HCPT.[29,30]

To examine the pharmacological activity of MWNTs **3** and the potential toxicity of the plain MWNTs (MWNTs **2**), the *in vitro* cytotoxicity of MWNTs **3** and **2** against MKN-28 cells was investigated together with a positive control of lyophilized clinical HCPT injection (Figure 6). The inhibitory ratio was determined after 48 h of incubation with a series of doses of HCPT injection, MWNTs **2** or **3** by WST-1 assay, since MTT assay, though generally used in cytotoxicity test, may give false results due to the interaction between CNTs and MTT-formazan

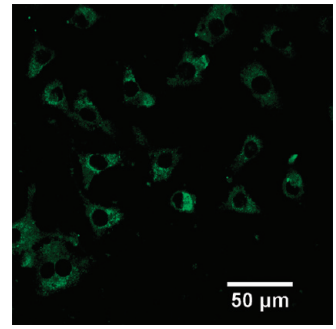

Figure 5. Typical fluorescence confocal microscopy image of MKN-28 cells incubated with 25 μg/mL of MWNTs 4 at 37 °C for 2 h.

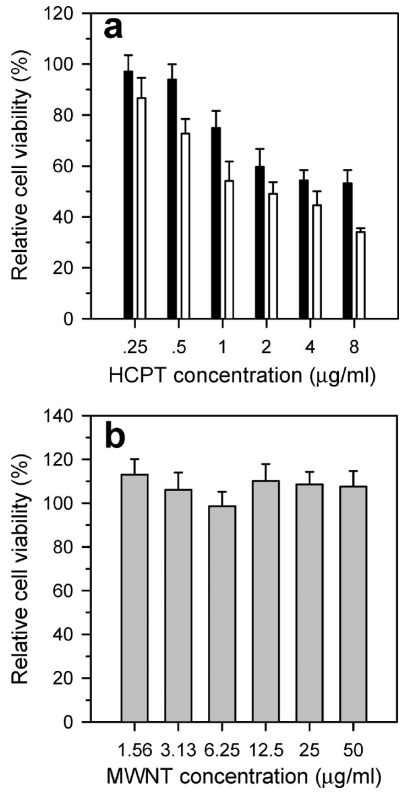

Figure 6. *In vitro* cytotoxicity of clinical HCPT injection (a, black), MWNTs 3 (a, white), and MWNTs 2 (b) against MKN-28 cells.

formed in the MTT reaction, which does not occur in the case of WST-1 assay.[31] As shown in Figure 6a, MWNTs **3** exhibit significantly improved cytotoxicity with respect to HCPT injection at equal HCPT concentrations, which may be associated with the enhanced cellular uptake of the drug by conjugation to CNTs as well as the multivalent presentation of HCPT on a single nanotube, acting as a drug concentrator. Furthermore, this study also confirms that the conjugation does not adversely influence the activity of HCPT. Additionally, no significant cytotoxicity is observed with the plain CNTs (MWNTs **2**) at all used concentrations (Figure 6b).

Biodistribution of the MWNT—HCPT Conjugates. Investigations of the *in vivo* behavior of MWNTs **3** are required to further understand how the conjugates act in a living system. Generally, nanomaterials including CNTs in the circulatory system are susceptible to osponization-induced RES capture, leading to the increased accumulation in RES organs (*e.g.*, liver and spleen) and decreased blood circulation time, which interferes greatly with their enrichment in tumor *via* enhanced permeability and retention (EPR) effect and eventual therapeutic efficacy.[2,21−23] As mentioned above, PEGylation can ameliorate such performance of CNTs to some extent; however, it also unfavorably decreases their cellular uptake efficiency. We anticipate that a desirable balance between the circulation time and cellular uptake efficiency of the drug-bearing CNTs can be reached by our strategy since the efficient cellular uptake has been

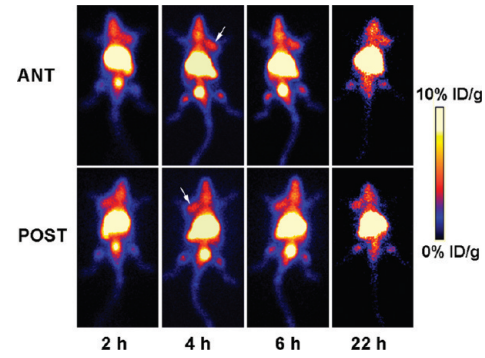

Figure 7. SPECT images of a hepatic H22 tumor-bearing mouse at various time points after injection of MWNTs 5 *via* the tail vein obtained from anterior (top) and posterior (bottom) acquisition under the anesthetized condition. The arrows denote the regions of the tumor.

proved as described above. To investigate the fate of MWNTs **3** in a living system using a radioactive tracing technique, the residual amino groups bound by MWNTs **3** (~0.13 mmol/g) were utilized to react with diethylenetriaminepentaacetic (DTPA) dianhydride followed by labeling with radioactive nuclide technetium-99m (^{99m}Tc; $T_{1/2}$ = 6.02 h, E_γ = 141 keV), affording MWNTs **5** (Scheme 1). The radioactive tracing is a straightforward and highly sensitive technique to probe quantitatively the *in vivo* behavior, and ^{99m}Tc is one of the most desirable nuclides due to its stable labeling and appropriate radiant energy. Thus, the sample of MWNTs **5** was used to investigate the fate in a living body.

SPECT imaging and gamma scintillation counting were used cooperatively to analyze the biodistribution of the ^{99m}Tc-labeled MWNT−HCPT (MWNTs **5**) injected into subcutaneous hepatic H22 tumor-bearing mice *via* the tail vein. Figure 7 displays the SPECT images of a hepatic H22 tumor-bearing mouse at various time points after the injection of MWNTs **5**. The different radioactive intensities are represented by different colors as shown in the color histogram in Figure 7. Briefly, the order of blue, red, yellow, and white corresponds to the successively increasing intensity. It can be seen from the images that MWNTs **5** are rapidly distributed throughout most tissues *via* blood circulation. In the whole region including lung, heart, liver, spleen, kidney, and stomach, strong signal can be observed. However, due to the planar image of the SPECT, the different organs in this region can hardly be distinguished. No significant intensity variation with time in this region is found within the monitoring period, indicating the relatively slow concentration change of MWNTs **5** in these organs. In contrast, the signal in the region of the intestine is relatively weak, and the weaker signal in the skin and muscle presents a striking contrast to the region of the head, tumor, femur, and other organs in the thoracic and abdominal cavities. Importantly, from the SPECT images, the enrichment of MWNTs **5** in the tumor is found over the whole experiment duration. The tumor is clearly visualized as pointed

by arrows in Figure 7, with signal intensity increasing from 2 to 4 h p.i. and then keeping roughly unchanged from 4 to 22 h p.i. In addition, a relatively strong signal can also be observed in the region of the bladder with time-dependent intensity, revealing that part of the injected MWNTs can be eliminated through the renal excretion route. As time elapsed, the signal intensity in this region increases initially and then becomes very weak at 22 h p.i. Considering the threshold of the glomerular filtration system, it can be speculated that only a fraction of nanotubes with very short length in MWNTs **5** sample can be excreted *via* the urinary route, which should occur at the early stage after administration because of the small percentage of this part.[22] Apart from the biodistribution investigations in mice, similar biodistribution patterns of MWNTs **5** injected into tumor-free rats *via* the tail vein were also obtained by SPECT imaging (see Figure S2 in Supporting Information).

In SPECT image, regions of interest can only present the total signal from all organs in the plane of projection due to the planar image, and thus these organs can hardly be analyzed individually. In view of this, the gamma scintillation counting analysis of dissected organs from hepatic H22 tumor-bearing mice was conducted at different time after injection of MWNTs **5** *via* the tail vein, which can precisely provide quantitative biodistribution of MWNTs **5** in different organs, compensating the shortage of the SPECT imaging. On the basis of the scintillation counting results in Figure 8, high uptake of MWNTs **5** was found in the liver, spleen, lung, kidney, stomach (emptied), femur, and tumor; in contrast, relatively low uptake was found in the heart, intestine (emptied), brain, skin, and muscle (thigh), which is well consistent with the results of SPECT imaging. As shown in Figure 8, the maximum levels of MWNTs **5** in liver and spleen among all of the test time points are about 25% injected dose (ID) per gram of wet tissue at 4 h p.i. and 16% ID/g at 6 h p.i., respectively. The high accumulations of MWNTs **5** in liver and spleen suggest that RES uptake occurred *via* blood circulation. Figure 9 gives the time-dependent variation of MWNTs **5** concentration in blood, tumor, and body of mice based on gamma scintillation counting. The half-life of MWNTs **5** in the blood circulation is calculated to be ~3.6 h (Figure 9a; see Methods and Experiments for the calculation method), longer than that of reported paclitaxel (PTX)-bearing PEGylated SWNTs (~1.1 h).[2] The dense hydrophilic short chain along the

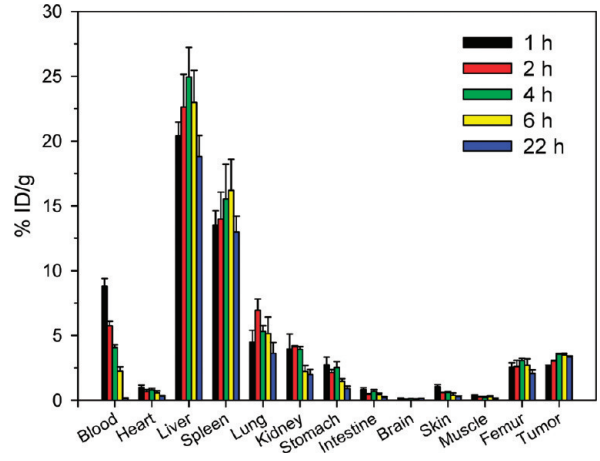

Figure 8. Biodistribution of MWNTs 5 in different organs of hepatic H22 tumor-bearing mice at various time points after tail vein injection. The values were acquired as the percentage of ID per gram of collected organs and based on five mice per group.

nanotubes should be responsible for this comparatively long circulation. Importantly, the rapid enrichment of MWNTs **5** in the tumor is also revealed quantitatively by the analyses of gamma scintillation counting. The tumor uptake of MWNTs **5** at 1 h p.i. is calculated to be ~2.7% ID/g. The maximum of tumor uptake among all of the test time points is found to be ~3.6% ID/g at 4 h p.i., and the level slightly decreased to ~3.3% ID/g at 22 h p.i. (Figure 9b), which corroborates the results of SPECT imaging. Furthermore, as shown in Figure 9c, there is still ~64% ID remaining in the body of mice at 22 h p.i., suggesting the

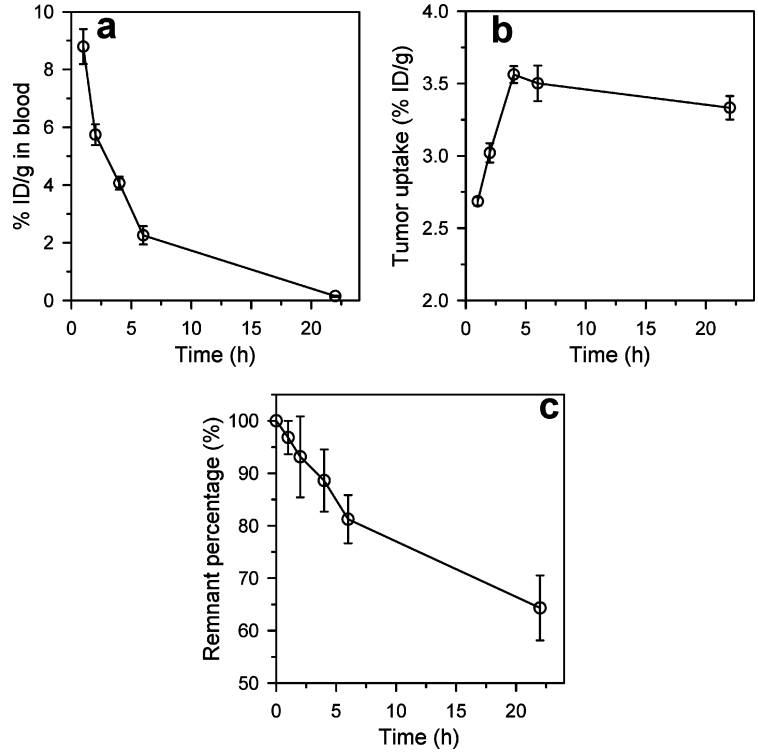

Figure 9. Variation of radiant activity in blood (a), tumor (b), and body of mice (c) at different time points p.i. expressed as the percentage of ID per gram of collected tissues (a,b) and the percentage of ID left in body (c). Data are presented as mean ± SD (n = 5).

slow excretion of MWNTs **5**, which is consistent with previous reports.[2,21−23]

Considering the HCPT release from the conjugates, HCPT may exhibit different distribution patterns compared to MWNTs **5** to some extent. However, on the basis of the *in vitro* HCPT release behavior of MWNTs **3** in FBS at 37 °C (Figure 4), which shows that only ~12% of the loaded HCPT is released from MWNTs **3** within 4 h incubation in the serum, it is reasonable to say that the half-life of MWNTs **5** in blood circulation (~3.6 h) basically reflects that of HCPT and the injected carbon nanotubes were taken up by various tissues with most HCPT conjugated since the maximum levels of MWNTs **5** in the tested tissues are essentially reached within 4 h p.i. except for spleen (reaching a maximum MWNTs **5** level at 6 h p.i.), as shown in Figure 8. What deserves to be mentioned is that carbon nanotubes were also taken up by tumor mostly in the conjugate form because MWNTs **5** reach a maximum level in the tumor within 4 h p.i. (Figure 9b), which is very important for the antitumor efficiency of MWNT−HCPT.

***In Vivo* Antitumor Performance and Toxicity of the MWNT−HCPT Conjugates.** The *in vivo* antitumor performance of MWNTs **3** was further investigated by using described subcutaneous hepatic H22 tumor-bearing mice as the model animals and was compared with that of clinical HCPT injection with two doses normalized to be 2.5 and 5 mg of HCPT equivalent (equiv) per kilogram of body weight, respectively. MWNTs **2** (containing the same nanotube concentration as MWNTs **3** with a dose of 5 mg/kg HCPT equiv) and saline-treated groups were used as control. All of the samples were injected as a solution in 0.3 mL of saline. Fifteen day follow-up experiments were carried out after administrations. On the basis of the tumor volume measurements performed every other day (Figure 10a), it can be observed that MWNTs **3** inhibited tumor growth much more efficiently than HCPT injection. Both the two HCPT formulations (MWNT−HCPT and HCPT injection) exhibit dose-dependent antitumor features, that is, the higher the drug dose, the better the antitumor activity. The group treated with MWNTs **3** at a dosage of 2.5 mg/kg HCPT equiv shows similar tumor suppression effect to the group treated with HCPT injection at the dose of 5 mg/kg HCPT equiv in the initial 9 days, but better effect from 9th to 15th day, which further confirms the better antitumor activity of MWNTs **3** than HCPT injection. The tumor growth inhibitions (TGI) calculated for the groups treated with MWNTs **3** at the doses of 5 and 2.5 mg/kg HCPT equiv are 64.3 and 48.5%, respectively, on the 15th day (see Methods and Experiments for the calculation method). In contrast, the TGI obtained from the groups treated with HCPT injection at doses of 5 and 2.5 mg/kg HCPT equiv are 32.4 and 18.1%, respectively, much lower than that of the group treated with MWNTs **3**. In addition, it is also found that MWNTs **2** have negligible inhibition effect.

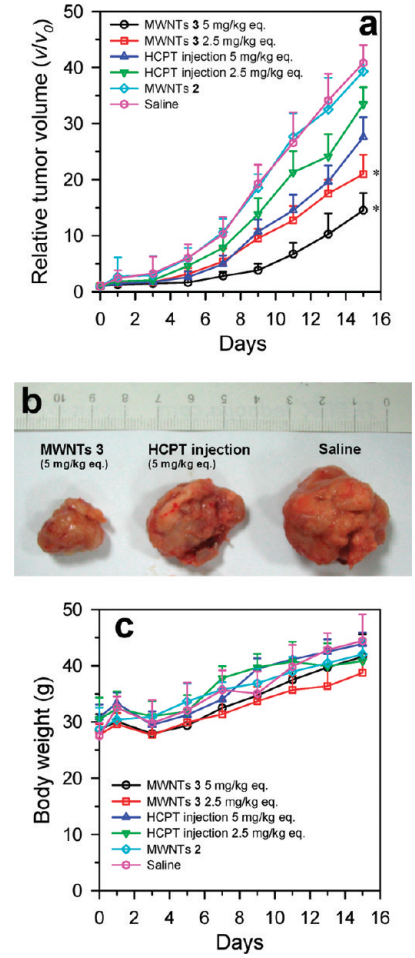

Figure 10. (a) *In vivo* antitumor effect obtained from each treated group, expressed as the average values of the relative tumor volume v/v_0 (where v denotes the tumor volume at test time points and v_0 denotes the corresponding initial tumor volume at the beginning of treatment). *$P < 0.05$ (*versus* HCPT injection group at the equivalent dose from the 5th day). (b) Typical photographs of excised sarcomas from mice on the 16th day after treatments with MWNTs 3 (5 mg/kg equiv), HCPT injection (5 mg/kg equiv), and saline. (c) Evolution of body weight of each group during the experiments. Data in a and c are presented as mean ± SD ($n = 8$).

The distinct inhibition effects can also be illustrated by the intuitive evidence from the representative photographs of excised sarcomas (Figure 10b). Over the course of the study, the weights (Figure 10c) and clinical situations of all the tested groups were scrutinized, which did not appear to be influenced by the treatments of either the two formulations of HCPT or the plain MWNTs when compared to the saline-treated group, indicating the well-tolerated dose levels of drug and the negligible toxicity of MWNTs imposed on the experimental mice.

To evaluate the necrosis level in the tumors from the groups treated with MWNTs **3** (5 mg/kg equiv), HCPT injection (5 mg/kg equiv), MWNTs **2**, and saline, the tumors were resected from the mice of the experimental groups after the 15 day treatments, and tumor slices stained by hematoxylin and eosin (H&E) were

analyzed *via* optical microscopy. Qualitatively, necrotic rate in the MWNTs **3**-treated tumor is explicitly highest among all of the tested groups. As shown by Figure 11, the large-area necrotic region can be observed in the MWNTs **3**-treated tumor. In contrast, the HCPT injection-treated tumors display a much lower necrotic level with a large amount of living cells existing, and the approximate level can be seen in either MWNTs **2** or saline-treated tumors. These results confirmed the superior treatment efficiency of MWNTs **3**.

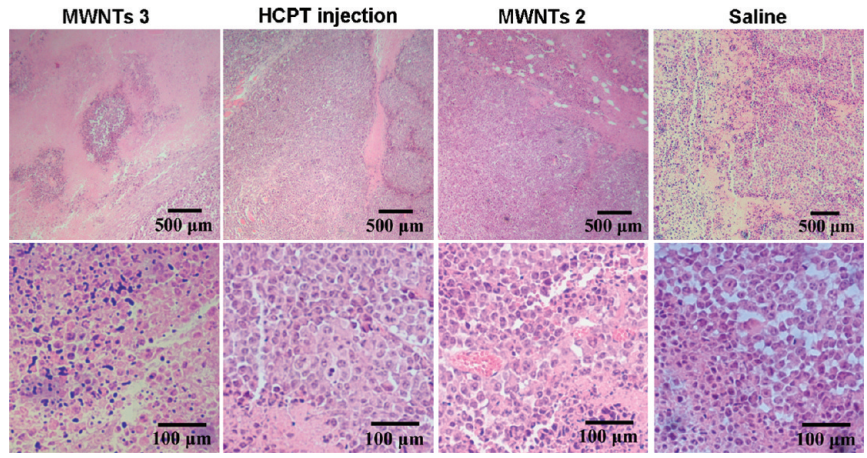

Figure 11. H&E stained tumor slices from mice on the 16th day after treatments with MWNTs 3 (5 mg/kg equiv), HCPT injection (5 mg/kg equiv), MWNTs 2, and saline.

The comparatively high accumulation of MWNTs **5** in some organs, including liver, spleen, lung, and kidney, urge us to further consider the potential pathological lesions induced by our samples on such organs. Histological analyses of the groups treated with MWNTs **3** (5 mg/kg equiv), HCPT injection (5 mg/kg equiv), MWNTs **2**, and saline were conducted at the completion of the 15 day tumor suppression study. As shown in Figure 12, histological slices in liver, spleen, lung, and kidney reveal that all of the samples of MWNTs **2** and **3** and HCPT injection do not cause any significant lesion to the tested organs, though some aggregates of CNTs can be observed in the slices of liver and spleen from the groups treated with MWNTs **2** and **3**, suggesting the low toxicity of MWNT−HCPT even to the high CNT-uptake organs at least in short-term, which can rationally be attributed to the relatively rapid release of HCPT *via* the cleavage of the ester linkage with the aid of esterase in these organs and subsequent rapid excretion of the disassociated HCPT with respect to the slow excretion of CNT-containing conjugates.[2] This would reduce the organs' exposure to HCPT and thus explain reasonably the harmlessness of the MWNTs **3** to the tested organs.

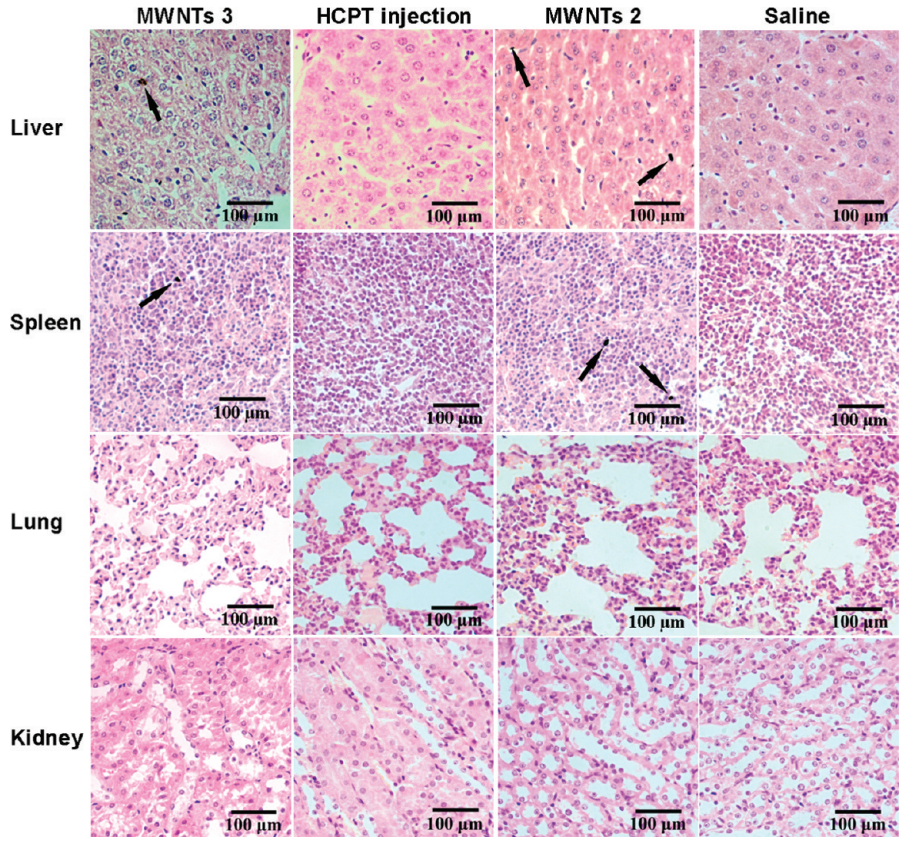

Figure 12. H&E stained liver, spleen, lung, and kidney slices from mice on the 16th day after treatments with MWNTs 3 (5 mg/kg equiv), HCPT injection (5 mg/kg equiv), MWNTs 2, and saline. The arrows point to the aggregates of CNTs in the slices of liver and spleen.

Combination of HCPT with CNTs can give great impact to the pharmacokinetic profiles of the drug as well as its cellular uptake efficiency, which should be the essential reasons for the superior antitumor effect of CNT-carried HCPT compared to its native formulation. As mentioned above, the half-life of MWNTs **5** in blood circulation is about 3.6 h *versus* 30 min of the blood circulation half-life of clinical HCPT injection in mice reported previously.[32] The prolonged blood circulation time of the drug is pivotal to improve its tumor accumulation and ultimate bioavailability.

Apart from the well-documented ability of CNTs to facilely penetrate the cell membrane,[1] it has been demonstrated by a very recent work that the intracellular

SWNTs can be released out of the cell renewedly.[33] This property may make it possible for the nanovehicles to translocate all over the whole tumor tissue, which has not been proved experimentally yet; nonetheless, it can be a possible source of the enhanced *in vivo* antitumor performance of the conjugated drug. Besides aforementioned factors, the multivalent presentation of HCPT molecules on a single nanotube should also be contributive to the therapeutic efficacy of MWNTs **3** that can be looked at as a concentrator of HCPT.

CONCLUSIONS

A water-soluble conjugate of MWNT−HCPT was synthesized by covalently linking HCPT to MWNTs with a hydrophilic molecule of diaminotriethylene glycol as the spacer between the two moieties following the derivation of HCPT with succinic anhydride at the 10-hydroxy position, by which a cleavable ester linkage was introduced and a drug loading of 16% of the MWNT−HCPT conjugates was obtained. The confocal microscopy, SPECT imaging, and gamma scintillation counting analyses revealed that the conjugates could be readily internalized by cells *in vitro* and exhibited relatively long blood circulation and high tumor accumulation *in vivo*. The *in vivo* tumor inhibition experiments confirmed the superior antitumor effect of the conjugates in comparison to its native formulation (clinical HCPT injection) and low toxicity to the living mice. The superior antitumor effect of the conjugates is ascribable to the enhanced cellular uptake efficiency, prolonged blood circulation, and HCPT-concentrating action (multivalent presentation of HCPT molecules on a single nanotube) of the conjugates. It is reasonable to say that this study provides an alternative practical and effective strategy for conjugating antitumor drugs to CNTs with great application potentials, which can be readily extended to other kinds of drugs or biomolecules.

METHODS AND EXPERIMENTS

General. Multiwalled carbon nanotubes (MWNTs) were purchased from Shenzhen Nanotech Port Co., Ltd. (Shenzhen, China). 10-Hydroxycamptothecin (HCPT) was kindly provided by Shanghai Institute of Materia Medica, Chinese Academy of Sciences. Lyophilized clinical HCPT injection was purchased from Shenzhen Main Luck Pharmaceuticals Inc. 2,2′-(Ethylenedioxy)-diethylamine, di-*tert*-butyl dicarbonate, *N*-(3-dimethylaminopropyl)-*N*′-ethylcarbodiimide hydrochloride (EDC × HCl), and *N*-hydroxysuccinimide (NHS) were purchased from Aldrich. FBS was obtained from Shanghai Luoshen Biotech Co., Ltd. (Shanghai, China). SEM analyses were conducted on HITACHI S-4800 at an accelerating voltage of 15 kV. UV−vis spectra were recorded on Shimadzu UV-2401 spectrophotometer. ^{1}H and ^{13}C NMR spectra were measured on a Bruker DRX 500 spectrometer. ESI-MS spectrometric data were determined with a LCQ ESI-MS Therso Finnigan mass spectrometer. XPS spectra were recorded on ESCALB MK-II, VG. High-performance liquid chromatographic (HPLC) analyses were performed on a Shimadzu LC-10AD (Shimadzu, Japan) HPLC system equipped with a Shimadzu RF-530 fluorescence detector and a Lichrospher C-18, 5 μm, 200 mm × 4.6 mm RP-HPLC analytical column. SPECT imaging was conducted on a Philips Skylight gamma camera. The radioactivity was measured by a NaI(T1) scintillor.

Synthesis. The experimental details for the synthesis of *d*-HCPT and all functionalized MWNTs can be found in the Supporting Information.

***In Vitro* Release of MWNTs 3 in Buffer Solutions.** MWNTs **3** bearing 40 μg of HCPT were dispersed in 0.5 mL of release medium with a specific pH value. The resulting solution was dialyzed against 20 mL of corresponding release medium in a 12 kDa MWCO membrane (Sigma, USA) at 37 °C with gentle agitation for 128 h. During this course, aliquots (1 mL) were taken from the outer medium at predetermined time points, and then the same volume of fresh medium was replenished immediately. The parts taken out were acidified with 20 μL of glacial acetic acid and stored at −20 °C until analysis by HPLC. Two release media including phosphate buffered saline (pH 7.4, 0.1 M) and acetate buffered saline (pH 5.0, 0.1 M) were used to understand the pH influence on the release profile. For the HPLC analyses of HCPT, a mobile phase of methanol/deionized water (75/25, v/v, pH = 5, adjusted with acetic acid) was used with a flow rate of 1.0 mL/min and column temperature at 35 °C. An excitation wavelength of 385 nm and an emission wavelength of 530 nm were applied for HCPT detection. The concentration of HCPT was determined based on the peak area at the retention time of ~2.7 min by reference to a calibration curve.

***In Vitro* Release of MWNTs 3 in Fetal Bovine Serum.** Fifty microliters of a saline solution of MWNTs **3** (bearing 15 μg of HCPT) was added in 5 mL of FBS. The resulting solution was incubated at 37 °C with gentle agitation for 128 h. During this course, aliquots (0.5 mL) were taken at predetermined time points. The parts taken out were acidified with 10 μL of glacial acetic acid and stored at 4 °C for 1 h to re-form the lactone ring of HCPT. To precipitate proteins and extract HCPT, 990 μL of acetonitrile/methanol (1/1, v/v, −20 °C) was added. Vortexed for 3 min and centrifuged at 12 000 rpm for 10 min, the supernatant was transferred to a glass vial and stored at −20 °C immediately until HPLC analysis. The mobile phase for HPLC analyses was a mixture of acetonitrile/aqueous buffer (40/60, v/v), in which the aqueous buffer contained 75 mmol/L ammonium acetate, 5 mmol/L triethylamine, and 0.5% (v/v) acetic acid. The retention time of HCPT was ~3.9 min. All of the other parameters were the same as described in the previous paragraph. The concentration of HCPT was determined based on the peak area by reference to a calibration curve.

***In Vitro* Cytotoxicity of MWNTs 3.** Cytotoxicity of MWNTs **3** against human gastric carcinoma cell line MKN-28 was studied in comparison with HCPT injection and plain MWNTs (MWNTs **2**). The cells were co-incubated with a series of doses of HCPT injection, MWNTs **3**, or MWNTs **2** at 37 °C for 48 h. Cell viability was tested by WST-1 assay, and the results were expressed as the viable percentage of cells after various treatments relative to the control cells without treatment.

Biodistribution Investigations of MWNTs 5. All animal experiments were performed in compliance with guidelines set by the Animal Care Committee at Drum Tower Hospital. To establish the experimental model of the tumor, H22 tumor cells ($5-6 \times 10^6$ cells per mouse) were inoculated subcutaneously into the armpit of ICR mice (6−8 weeks, 22−26 g).

For the biodistribution experiments, 0.3 mL of a saline solution of ^{99m}Tc-labeled MWNT−HCPT conjugates (MWNTs **5**) at the dosage of 5 mg/kg HCPT equiv with 300 μCi of ^{99m}Tc was injected to the tail vein of H22 tumor-bearing mice on the sixth day after inoculation. Three mice were used to perform SPECT imaging on a Philips Skylight gamma camera under the anesthetized condition.

For gamma scintillation counting, the mice administrated as described in last paragraph were sacrificed at 1, 2, 4, 6, and 22 h post injection with five mice for one time point. The blood of

each mouse was collected from the ophthalmic artery, and subsequently, the tissues including the heart, liver, spleen, lung, kidney, stomach (emptied), intestine (emptied), brain, skin, muscle (thigh), femur, and tumor were excised. After a rinse in deionized water and removal of the exterior water with filter paper carefully, the tissues were put into preweighed vials and counted for ^{99m}Tc activity by a γ-counter. An identical sample to that injected was also counted at each time point as a reference to eliminate the interference of the physical decay of radioactivity. The distribution results were defined as the percentage of injected dose per gram of wet tissues (% ID/g).

The blood circulation half-life ($t_{1/2}$) was calculated on the basis of the first-order exponential decay fitting of concentration−time data with the following equation:

$$C = C_0 \times e^{-kt}$$

where C denotes the blood concentration; C_0 is the initial blood concentration; t is the time after injection; and k is the elimination constant. Then, the blood circulation half-life was obtained by $t_{1/2} = \ln 2/k$.

In addition, the biodistribution of MWNTs **5** in a tumor-free rat was also studied primarily by SPECT imaging. In this experiment, 0.5 mL of a saline solution of MWNTs **5** (about 1 mg) with 500 μCi of ^{99m}Tc was injected to the tail vein of a tumor-free rat. Three rats were used to perform SPECT imaging on a Philips Skylight gamma camera under the anesthetized condition.

***In Vivo* Tumor Inhibition of MWNTs 3.** The tumor models were established by inoculating subcutaneously H22 tumor cells (5−6 × 10^6 cells per mouse) into the armpit of ICR mice (6−8 weeks, 22−26 g) as mentioned above. When the tumor reached a mean volume of ~300 mm^3 (6 days after inoculation), the mice were randomly divided into six groups (eight per group) and then injected *via* tail vein with 0.3 mL solution of different formulations of HCPT (MWNTs **3** and lyophilized clinical HCPT injection) and MWNTs **2** in saline and neat saline (0.3 mL, as negative control), respectively. Both of the formulations of HCPT were injected at two doses normalized to be 2.5 and 5 mg/kg HCPT equiv, respectively. The injected MWNTs **2** contain the same amount of nanotubes as the higher dose of MWNTs **3** (about 27 mg/kg). After the administration, 15 day follow-up experiments were performed, in which tumor sizes were measured by vernier calipers on an alternate day and calculated as volume $V = d^2 \times D/2$ (where d and D denote the shortest and longest diameter of the tumor in mm, respectively), and the weights and clinical situations of all the tested mice were also scrutinized.

The tumor growth inhibition (TGI) was calculated by the following equation:

$$\mathrm{TGI} = \frac{\bar{V}\text{ of saline control group} - \bar{V}\text{ of tested group}}{\bar{V}\text{ of saline control group}} \times 100\%$$

where $\bar{V}$ is the average tumor volume.

Histology Study. On the 16th day after treatment, the tissues including tumor, liver, spleen, lung, and kidney from the test groups treated with MWNTs **3** (5 mg/kg equiv), HCPT injection (5 mg/kg equiv), MWNTs **2**, and saline were dissected and fixed in 10% neutral buffered formalin. The tissues were processed routinely into paraffin, sectioned at a thickness of 4 μm, stained with hematoxylin and eosin (H&E), and examined by optical microscopy.

Statistical Analysis. Student's t-test was used to determine the difference of tumor inhibition between the groups treated with MWNTs **3** and HCPT injection at the equivalent dose of HCPT, and P values less than 0.05 were considered statistically significant.

Acknowledgment. This research project has been supported by the Natural Science Foundation of China (Nos. 50802040, 50625311, 20874042) and the Ph.D. Programs Foundation of Ministry of Education of China (No. 200802841037).

Supporting Information Available: Experimental details for the synthesis of *d*-HCPT and all functionalized MWNTs and SPECT images of a tumor-free rat at various time points after injection of MWNTs **5** *via* tail vein. This material is available free of charge *via* the Internet at http://pubs.acs.org.

REFERENCES AND NOTES

1. Lu, F.; Gu, L.; Meziani, M. J.; Wang, X.; Luo, P. G.; Veca, L. M.; Cao, L.; Sun, Y.-P. Advances in Bioapplications of Carbon Nanotubes. *Adv. Mater.* **2009**, *21*, 139–152.
2. Liu, Z.; Chen, K.; Davis, C.; Sherlock, S.; Cao, Q.; Chen, X.; Dai, H. Drug Delivery with Carbon Nanotubes for *In Vivo* Cancer Treatment. *Cancer Res.* **2008**, *68*, 6652–6660.
3. Dhar, S.; Liu, Z.; Thomale, J.; Dai, H.; Lippard, S. J. Targeted Single-Wall Carbon Nanotube-Mediated Pt(IV) Prodrug Delivery Using Folate as a Homing Device. *J. Am. Chem. Soc.* **2008**, *130*, 11467–11476.
4. Liu, Z.; Sun, X.; Nakayama-Ratchford, N.; Dai, H. Supramolecular Chemistry on Water-Soluble Carbon Nanotubes for Drug Loading and Delivery. *ACS Nano* **2007**, *1*, 50–56.
5. Feazell, R. P.; Nakayama-Ratchford, N.; Dai, H.; Lippard, S. J. Soluble Single-Walled Carbon Nanotubes as Longboat Delivery Systems for Platinum(IV) Anticancer Drug Design. *J. Am. Chem. Soc.* **2007**, *129*, 8438–8439.
6. Bhirde, A. A.; Patel, V.; Gavard, J.; Zhang, G.; Sousa, A. A.; Masedunskas, A.; Leapman, R. D.; Weigert, R.; Gutkind, J. S.; Rusling, J. F. Targeted Killing of Cancer Cells *In Vivo* and *In Vitro* with EGF-Directed Carbon Nanotube-Based Drug Delivery. *ACS Nano* **2009**, *3*, 307–316.
7. Chen, J.; Chen, S.; Zhao, X.; Kuznetsova, L. V.; Wong, S. S.; Ojima, I. Functionalized Single-Walled Carbon Nanotubes as Rationally Designed Vehicles for Tumor-Targeted Drug Delivery. *J. Am. Chem. Soc.* **2008**, *130*, 16778–16785.
8. Ali-Boucetta, H.; Al-Jamal, K. T.; McCarthy, D.; Prato, M.; Bianco, A.; Kostarelos, K. Multiwalled Carbon Nanotube−Doxorubicin Supramolecular Complexes for Cancer Therapeutics. *Chem. Commun.* **2008**, 459–461.
9. Welsher, K.; Liu, Z.; Daranciang, D.; Dai, H. Selective Probing and Imaging of Cells with Single Walled Carbon Nanotubes as Near-Infrared Fluorescent Molecules. *Nano Lett.* **2008**, *8*, 586–590.
10. Liu, Z.; Li, X.; Tabakman, S. M.; Jiang, K.; Fan, S.; Dai, H. Multiplexed Multicolor Raman Imaging of Live Cells with Isotopically Modified Single Walled Carbon Nanotubes. *J. Am. Chem. Soc.* **2008**, *130*, 13540–13541.
11. Kam, N. W. S.; Liu, Z.; Dai, H. Functionalization of Carbon Nanotubes *via* Cleavable Disulfide Bonds for Efficient Intracellular Delivery of siRNA and Potent Gene Silencing. *J. Am. Chem. Soc.* **2005**, *127*, 12492–12493.
12. Kam, N. W. S.; Jessop, T. C.; Wender, P. A.; Dai, H. Nanotube Molecular Transporters: Internalization of Carbon Nanotube−Protein Conjugates into Mammalian Cells. *J. Am. Chem. Soc.* **2004**, *126*, 6850–6851.
13. Cherukuri, P.; Bachilo, S. M.; Litovsky, S. H.; Weisman, R. B. Near-Infrared Fluorescence Microscopy of Single-Walled Carbon Nanotubes in Phagocytic Cells. *J. Am. Chem. Soc.* **2004**, *126*, 15638–15639.
14. Cherukuri, P.; Gannon, C. J.; Leeuw, T. K.; Schmidt, H. K.; Smalley, R. E.; Curley, S. A.; Weisman, R. B. Mammalian Pharmacokinetics of Carbon Nanotubes Using Intrinsic Near-Infrared Fluorescence. *Proc. Natl. Acad. Sci. U.S.A.* **2006**, *103*, 18882–18886.
15. Gannon, C. J.; Cherukuri, P.; Yakobson, B. I.; Cognet, L.; Kanzius, J. S.; Kittrell, C.; Weisman, R. B.; Pasquali, M.; Schmidt, H. K.; Smalley, R. E.; et al. Carbon Nanotube-Enhanced Thermal Destruction of Cancer Cells in a Noninvasive Radio Frequency Field. *Cancer* **2007**, *110*, 2654–2665.
16. Pastorin, G.; Wu, W.; Wieckowski, S.; Briand, J.-P.; Kostarelos, K.; Prato, M.; Bianco, A. Double Functionalisation of Carbon Nanotubes for Multimodal Drug Delivery. *Chem. Commun.* **2006**, 1182–1184.
17. Wu, W.; Wieckowski, S.; Pastorin, G.; Benincasa, M.; Klumpp, C.; Briand, J.-P.; Gennaro, R.; Prato, M.; Bianco, A. Targeted Delivery of Amphotericin B to Cells by Using Functionalized Carbon Nanotubes. *Angew. Chem., Int. Ed.* **2005**, *44*, 6358–6362.

18. Schipper, M. L.; Nakayama-Ratchford, N.; Davis, C. R.; Kam, N. W. S.; Chu, P.; Liu, Z.; Sun, X. M.; Dai, H.; Gambhir, S. S. A Pilot Toxicology Study of Single-Walled Carbon Nanotubes in a Small Sample of Mice. *Nat. Nanotechnol.* **2008**, *3*, 216–221.
19. Yang, S.-T.; Wang, X.; Jia, G.; Gu, Y.; Wang, T.; Nie, H.; Ge, C.; Wang, H.; Liu, Y. Long-Term Accumulation and Low Toxicity of Single-Walled Carbon Nanotubes in Intravenously Exposed Mice. *Toxicol. Lett.* **2008**, *181*, 182–189.
20. Zerda, A. D. L.; Zavaleta, C.; Keren, S.; Vaithilingam, S.; Bodapati, S.; Liu, Z.; Levi, J.; Smith, B. R.; Ma, T.-J.; Oralkan, O.; *et al.* Carbon Nanotubes as Photoacoustic Molecular Imaging Agents in Living Mice. *Nat. Nanotechnol.* **2008**, *3*, 557–562.
21. Liu, Z.; Cai, W.; He, L.; Nakayama, N.; Chen, K.; Sun, X.; Chen, X.; Dai, H. *In Vivo* Biodistribution and Highly Efficient Tumour Targeting of Carbon Nanotubes in Mice. *Nat. Nanotechnol.* **2007**, *2*, 47–52.
22. Liu, Z.; Davis, C.; Cai, W.; He, L.; Chen, X.; Dai, H. Circulation and Long-Term Fate of Functionalized, Biocompatible Single-Walled Carbon Nanotubes in Mice Probed by Raman Spectroscopy. *Proc. Natl. Acad. Sci. U.S.A.* **2008**, *105*, 1410–1415.
23. Yang, S. T.; Fernando, K. A. S.; Liu, J.-H.; Wang, J.; Sun, H.-F.; Liu, Y.; Chen, M.; Huang, Y.; Wang, X.; Wang, H.; *et al.* Covalently PEGylated Carbon Nanotubes with Stealth Character *In Vivo*. *Small* **2008**, *4*, 940–944.
24. Hamad, I.; Hunter, A. C.; Szebeni, J.; Moghimi, S. M. Poly(ethylene glycol)s Generate Complement Activation Products in Human Serum through Increased Alternative Pathway Turnover and a MASP-2-Dependent Process. *Mol. Immunol.* **2008**, *46*, 225–232.
25. Moghimi, S. M.; Szebeni, J. Stealth Liposomes and Long Circulating Nanoparticles: Critical Issues in Pharmacokinetics, Opsonization and Protein-Binding Properties. *Prog. Lipid Res.* **2003**, *42*, 463–478.
26. Szebeni, J. Complement Activation-Related Pseudoallergy Caused by Liposomes, Micellar Carriers of Intravenous Drugs, and Radiocontrast Agents. *Crit. Rev. Ther. Drug Carrier Syst.* **2001**, *18*, 567–606.
27. Liu, Z.; Winters, M.; Holodniy, M.; Dai, H. siRNA Delivery into Human T Cells and Primary Cells with Carbon-Nanotube Transporters. *Angew. Chem., Int. Ed.* **2007**, *46*, 2023–2027.
28. Zeineldin, R.; Al-Haik, M.; Hudson, L. G. Role of Polyethylene Glycol Integrity in Specific Receptor Targeting of Carbon Nanotubes to Cancer Cells. *Nano Lett.* **2009**, *9*, 751–757.
29. Jaxel, C.; Kohn, K. W.; Wani, M. C.; Wall, M. E.; Prommier, Y. Structure−Activity Study of the Actions of Camptothecin Derivatives on Mammalian Topoisomerase I: Evidence for a Specific Receptor Site and a Relation to Antitumor Activity. *Cancer Res.* **1989**, *49*, 1465–1469.
30. Carbonero, R.; Supko, J. Current Perspectives on the Clinical Experience, Pharmacology, and Continued Development of the Camptothecins. *Clin. Cancer Res.* **2002**, *8*, 641–661.
31. Wörle-Knirsch, J. M.; Pulskamp, K.; Krug, H. F. Oops They Did It Again! Carbon Nanotubes Hoax Scientists in Viability Assays. *Nano Lett.* **2006**, *6*, 1261–1268.
32. Zhang, X.; Gan, Y.; Yang, X.; Zhu, C.; Gan, L.; Nie, S.; Pan, W. Preparation of PEG-Modified Nanostructured Lipid Carriers Loaded with Hydroxycamptothecin and Tissue Distribution in Mice. *Acta Pharm. Sinica* **2008**, *43*, 91–96.
33. Cheng, J.; Fernando, K. A. S.; Veca, L. M.; Sun, Y.-P.; Lamond, A. I.; Lam, Y. W.; Cheng, S. H. Reversible Accumulation of PEGylated Single-Walled Carbon Nanotubes in the Mammalian Nucleus. *ACS Nano* **2008**, *2*, 2085–2094.